Modelling the Insect Navigation Toolkit: How the Mushroom Bodies and Central Complex Coordinate Guidance Strategies

Xuelong Sun[1], **Shigang Yue**[1†], **Michael Mangan**[2†]

[1]Computational Intelligent Lab, School of Computer Science, University of Lincoln, Lincoln, United Kingdom; [2]Sheffield Robotics, Department of Computer Science, University of Sheffield, Sheffield, United Kingdom

***For correspondence:**
syue@lincoln.ac.uk;
m.mangan@sheffield.ac.uk;
xsun@lincoln.ac.uk

[†]Joint last authorship

Abstract

The robust navigation of insects arises from the coordinated action of concurrently functioning and interacting guidance systems. Computational models of specific brain regions can account for isolated behaviours such as path integration or route following but the neural mechanisms by which their outputs are coordinated remains unknown. Here we take a functional modelling approach to identify and model the elemental guidance subsystems required by homing insects before producing realistic adaptive behaviours by integrating their outputs in a biologically constrained unified model mapped onto identified neural circuits. Homing paths are quantitatively and qualitatively compared with real ant data in a series of simulation studies replicating key infield experiments. Our analysis reveals that insects require independent visual homing and route following capabilities which we show can be realised by encoding panoramic skylines in the frequency domain, using image processing circuits in the optic lobe and learning pathways through the Mushroom Bodies and Anterior Optic Tubercle respectively before converging in the Central Complex steering circuit. Further we demonstrate that a ring-attractor network inspired by firing patterns recorded in the Central Complex can optimally integrate the outputs of path integration and visual homing systems guiding simulated ants back to their familiar route, and a simple non-linear weighting function driven by the output of the Mushroom Bodies provides a context-dependent switch allowing route following strategies to dominate and the learned route retraced back to the nest when familiar terrain is encountered. The outcome is a biologically realistic neural model capable of reproducing an array of adaptive homing behaviours in realistic environments through the combined action of the Central Complex and the Mushroom Bodies neuropils forwarding the case for a distributed architecture of the insect navigational toolkit.

Introduction

Central-place foraging insects (especially desert ant who relays little on pheromone) navigate using a 'toolkit' of independent guidance systems (***Wehner, 2009***) of which the most fundamental are path integration (PI), whereby foragers track the distance and direction to their nest by integrating the series of directions and distances travelled (for reviews see ***Heinze et al.*** (***2018***); ***Collett*** (***2019***)), and visual memory (VM), whereby foragers derive a homing signal by comparing the difference between current and stored views (for reviews see ***Zeil*** (***2012***); ***Collett et al.*** (***2013***)). Neurophysiological and

computational modelling studies advocate the central complex neuropil (CX) as the PI centre (***Heinze and Homberg, 2007***; ***Seelig and Jayaraman, 2015***; ***Stone et al., 2017***), whereas the mushroom body neuropils (MB) appear well suited to assessing visual valence as needed for VM (***Heisenberg, 2003***; ***Ardin et al., 2016***; ***Müller et al., 2018***). Yet, two key gaps in our understanding remain. Firstly, although current VM models based on the MB architecture can replicate route following (RF) behaviours (***Ardin et al., 2016***; ***Müller et al., 2018***) they cannot account for visual homing (VH) behaviours whereby insects return directly to their familiar surroundings from novel locations following a displacement (e.g. after being blown off course by a gust of wind) (***Wystrach et al., 2012***). Secondly, despite increasingly neuroanatomical evidence suggesting that premotor regions of the CX coordinate navigation behaviour (***Pfeiffer and Homberg, 2014***; ***Heinze and Pfeiffer, 2018***; ***Honkanen et al., 2019***), a theoretical hypothesis explaining how this is achieved by the neural circuitry has yet to be developed. In this work we develop a unified neural navigation model that extents the core guidance modules from two (PI and VM) to three (PI, RF, and VH) and by integrating their outputs optimally using biologically realistic models of the CX produces realistic homing behaviours.

The foremost challenge in realising this goal is to ensure that the core guidance subsystems provide sufficient directional information across conditions. Contemporary VM models based on the MBs can replicate realistic route following behaviours in complex visual environments (ant environments: ***Kodzhabashev and Mangan*** (***2015***); ***Ardin et al.*** (***2016***); bee environments: ***Müller et al.*** (***2018***)) but do not generalise to visual homing scenarios whereby the animal must return directly to familiar terrain from novel locations (ants: ***Narendra*** (***2007***), bees ***Cartwright and Collett*** (***1982***), wasps ***Stürzl et al.*** (***2016***)). Storing multiple nest-facing views before foraging, inspired by observed learning walks in ants (***Müller and Wehner, 2010***; ***Fleischmann et al., 2016***) and flights in bees and wasps (***Zeil et al., 1996***; ***Zeil and Fleischmann, 2019***), provides a potential solution (***Graham et al., 2010***; ***Wystrach et al., 2013***), but simulation studies have found this approach to be brittle due to high probabilities of aligning with the wrong memory causing catastrophic errors (***Dewar et al., 2014***). Moreover, ants released perpendicularly to their familiar route do not generally align with their familiar visual direction as predicted by the above algorithms (***Wystrach et al., 2012***), but instead move directly back towards the route (***Fukushi and Wehner, 2004***; ***Kohler and Wehner, 2005***; ***Narendra, 2007***; ***Mangan and Webb, 2012***; ***Wystrach et al., 2012***), which would require a multi-stage mental alignment of views for current models. New computational hypothesis are thus required that can guide insects directly back to their route (often moving perpendicularly to the habitual path), but also allow for the route direction to be recovered (now aligned with the habitual path) when within familiar surroundings (see ***Figure 1***A "Zero Vector").

With the necessary elemental guidance systems defined, a unifying model must then convert the various directional recommendations into a single motor command appropriate to the context (***Cruse and Wehner, 2011***; ***Hoinville et al., 2012***; ***Collett et al., 2013***; ***Webb, 2019***). Behavioural studies show that when in unfamiliar visual surroundings ("Off-Route") insects combine the outputs of their PI and VH systems (***Collett, 1996***; ***Bregy et al., 2008***; ***Collett, 2012***) relative to their respective certainties consistent with optimal integration theory (***Legge et al., 2014***; ***Wystrach et al., 2015***). In practice, this compromise leads ants to converge on their route but in a less direct manner (***Figure 1***A "Full Vector"). Upon encountering their familiar route, insects readily recognise their surroundings, recover their previous bearing and retrace their familiar path home (***Harrison et al., 1989***; ***Kohler and Wehner, 2005***; ***Wystrach et al., 2011***; ***Mangan and Webb, 2012***). Thus, the navigation coordination model must posses two capabilities: (a) output a directional signal consistent with the optimal integration of PI and VH when Off-Route (b) switch from Off-Route (PI and VH) to On-Route (RF) strategies when familiar terrain is encountered. Mathematical models have been developed that reproduce aspects of cue integration in specific scenarios (***Cruse and Wehner, 2011***; ***Hoinville and Wehner, 2018***), but to date no neurobiologically constrained network revealing how insects might realise these capabilities has been developed.

To address these questions a functional modelling approach is followed that extends to the

current base model described by (***Webb, 2019***) to (a) account for the ability of ants to home from novel locations back to the familiar route before retracing their familiar path the rest of the journey home, and (b) propose a neurally-based model of the central complex neuropil that integrates competing cues optimally and generates a simple steering command that can drive behaviour directly. Performance is bench-marked by direct comparison to behavioural data reported by ***Wystrach et al.*** (***2012***) (showing different navigation behaviours on and off the route), (***Legge et al., 2014***; ***Wystrach et al., 2015***) (demonstrating optimal integration of PI and VM), and through qualitative comparison to extended homing paths where insects switch between strategies according to the context (***Narendra, 2007***). Biological realism is enforced by constraining models to the known anatomy of specific brain areas, but where no data exists we take an exploratory approach to investigate the mechanisms that insects may exploit. ***Figure 1*** depicts the adaptive behaviours observed in animals that we wish to replicate and an overview of our unified model of insect navigation.

Results

Mushroom Bodies As Drivers of Rotational Invariant Visual Homing

To realise direct VH to the route without continuous mental or physical realignment we take inspiration from ***Stone et al.*** (***2018***) who demonstrated that panoramic skylines processed in the frequency domain, which naturally separates information into rotational-invariant **amplitudes** and rotationally-varying *phases*, provide sufficient information for rotational-invariant visual homing to a single target location.

The intensity sensitive input neurons of ***Ardin et al.*** (***2016***)'s MB model are replaced with input neurons encoding rotational invariant ***amplitudes*** (see Discussion ***section*** for biological plausibility). The network is trained along an $11m$ curved route in a simulated world that mimics the training regime of ants in (***Wystrach et al., 2012***) (see Methods ***subsection*** and Results ***subsection*** for details on simulated world, image processing, model architecture and training and test regime). After training, the firing rate of the mushroom body output neuron (MBON) when placed at locations across the environment at random orientations reveals a gradient that increases monotonically with distance from the familiar route area, providing a homing signal sufficient for VH independent of the animal's orientation (***Figure 2***C).

Motor output is generated by connecting the MBON to the recently discovered CX steering network (***Stone et al., 2017***) via the superior medial protocerebrum (SMP) (***Aso et al., 2014***; ***Plath et al., 2017***) which in our model responds only to positive increases in MBON activity (see ***Figure 2***A). The CX steering circuit, found in the fan-shape body (FB/CBU), minimises the offset between the animals current and a desired heading. In the proposed VH model the current heading is modelled as a sinusoidal activity profile in the ring of TB1 neurons found in the protocerebral bridge (PCB/PB) tracking the celestial compass as in ***Stone et al.*** (***2017***). The desired heading is derived by mirroring the current heading ring-network to a matched ring-network (assumed CPU3 neurons) but crucially with activity shifted leftwards in proportion to the increase MBON activity (provided by the SMP pathway). The result is a mechanism that iteratively refines the animals orientation to keep it moving down the gradient and thus back towards familiar terrain (***Figure 2***B).

Figure 2C demonstrates that the proposed network accurately replicates both the directed initial paths as in ***Wystrach et al.*** (***2012***) (see the inserted black arrow), and extended homing paths as in ***Narendra*** (***2007***) observed in ants displaced to novel locations perpendicular to their familiar routes. We note that upon encountering the route the model is unable to distinguish the direction in which to travel and thus meanders back and forth along the familiarity valley, unlike real ants, demonstrating the need for additional route recognition and recovery capabilities.

Optimally Integrating Visual Homing and Path Integration

We have demonstrated how ants could use visual cues to return to the route in the absence of PI but in most natural scenarios (e.g. displacement by a gust of wind) ants will retain a home

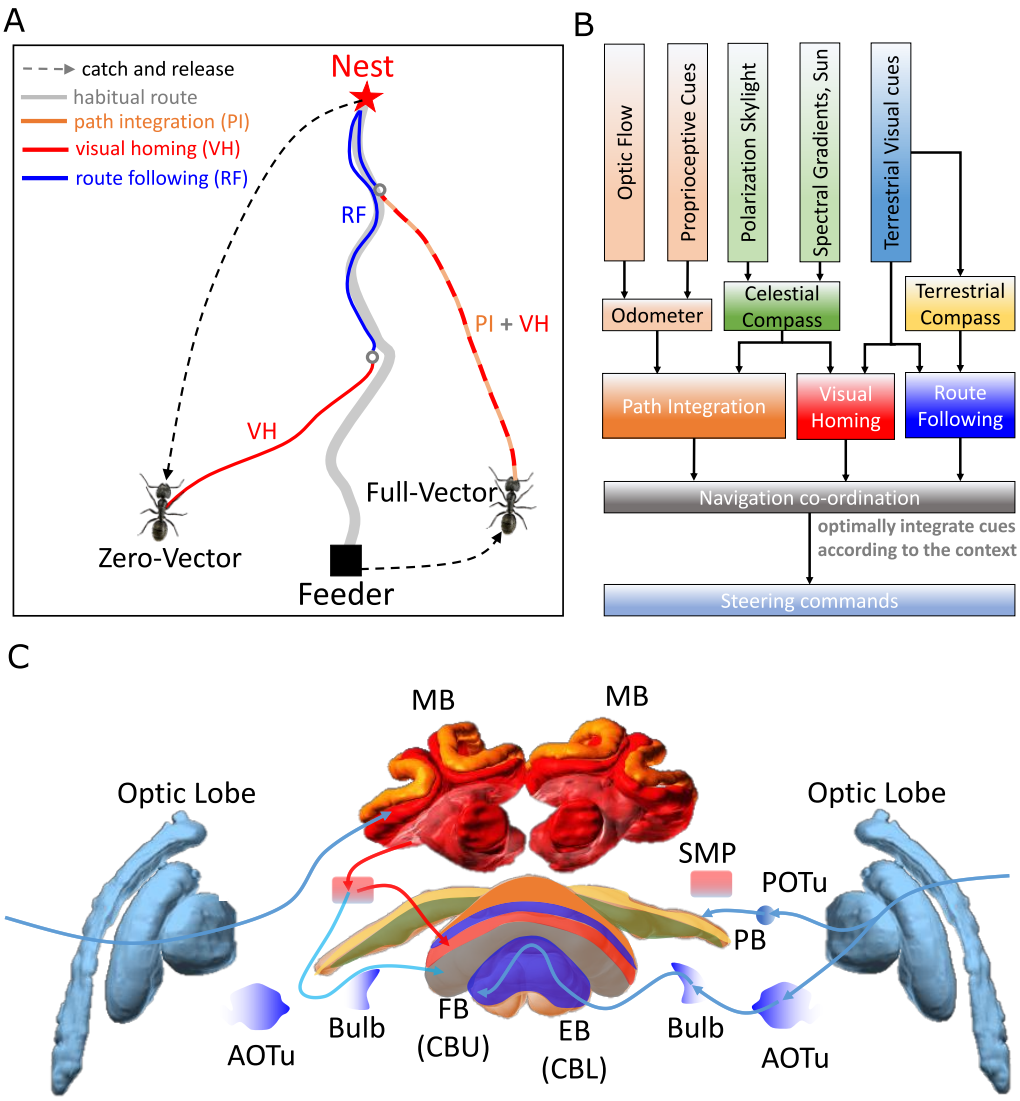

Figure 1. Overview of the unified navigation model and it's homing capabilities. (**A**) The homing capabilities produced by the model replicate the adaptive homing behaviour of insects with path integration and visual homing combined optimally to drive the animal back to familiar surroundings (banded red and green path segment) before the route is recognised and retraced home (blue path segment). (**B**) The proposed conceptual model of the insect navigation toolkit from sensory input to motor output. Three elemental guidance system are all modelled in this paper: path integration , visual homing (VH) and route following (RF) . Their outputs must then be coordinated in an optimal manner appropriate to the context as in insects. (**C**) The unified navigation model maps the elemental guidance systems to distinct processing pathways: ***RF***: optic lobe -> AuTo -> CX; ***VH***: optic lobe -> MB -> SMP -> CX; ***PI***: optic lobe -> CX. The outputs are then optimally integrated in the ring attractor networks of the FB in CX to generate a single motor steering command. Images of the brain regions are adapted from the insect brain database https://www.insectbraindb.org.

vector readout offering an alternative, and often conflicting, guidance cue to that provided by visual homing. In such scenarios desert ants strike a comprise by integrating their PI and VH outputs in a manner consistent with optimal integration theory by weighting VH relative to the familiarity of the current view (***Legge et al., 2014***) and PI relative to the home vector length (a proxy for directional certainty) (***Wystrach et al., 2015***).

Artificial ring-attractor networks, similar to those found in the CX (***Green et al., 2017***), output the

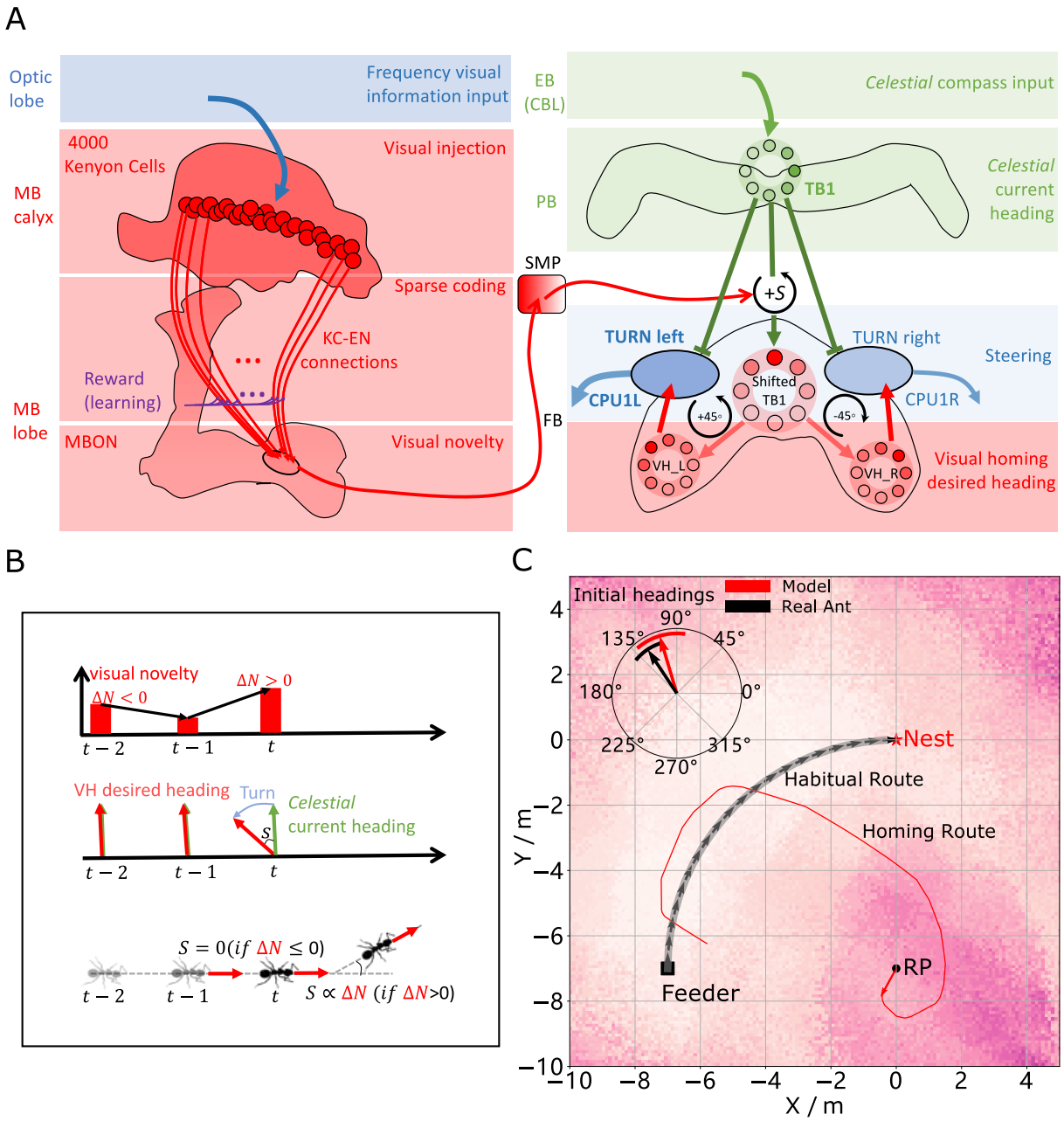

Figure 2. Visual Homing in the Insect Brain. (**A**) Proposed model of visual homing in the insect brain. Frequency encoded views arrive in the MB calyx then project to the sparse encoding in the Kenyon cells (KCs) before converging on the output neuron (MBON) that sums all activation in KCs via plastic connections. These connections are tuned through the reinforcement learning (more details see ***subsubsection***). The MBON indicating the visual novelty connects to the SMP which is activated by positive increases in MBON activity. SMP causes a shift in the activity profile from the current heading in the ring of cells indicating the VH desired heading of visual homing. The steering circuit compares the celestial compass (current heading) with the VH desired heading to generate the appropriate motor command. (**B**) Schematic diagram of the proposed visual homing model. For every time step from $t-2$ to t, the sensory data of visual novelty will drive the agent's motor to descent the visual novelty gradient. How this left turn is generated neurally is showni n A, where the desired heading is shifted 90 degrees from the current heading, leading to increased activity on in the turn left ring of the steering circuit. (**C**) Resultant visual homing behaviours as in (***Wystrach et al., 2012***). The grey curve shows the habitual route along which ants were trained. RP indicated the release point from which simulated and real ants were tested. The firing rate of the MBON sampled across locations at random orientation is depicted by the heat-map showing a clear gradient leading back to the route directly. The ability of the MB->SMP->CX model to generate realistic homing data in this scenario is shown by the initial paths of simulated ants which closely match those of real ants (see inserted polar plot), and also the extended homing path shown. Note that once the agent get the vicinity of the route, it will wandering around because of the flat of visual novelty gradient.

weighted sum of their inputs approximating optimal cue integration (***Touretzky, 2005***; ***Sun et al., 2018***) offering a biologically realistic means to weight PI and VH cues optimally. Thus a ring-attractor network is added to the CX model (see ***Figure 3***A) that takes as input the desired headings from the above proposed VH model and ***Stone et al.*** (***2017***)'s PI model and outputs a combined Off Route desired heading signal that is sent to the steering circuit. The certainty of PI automatically scales with the home-vector length owing to the accumulating effect of the memory neurons which correlates with directional uncertainty (***Wystrach et al., 2015***). In our implementation the VH input has a fixed height and width profile and influences the integration by tuning connections from the TN (see the plotted activation function in ***Figure 3***B and Method ***subsubsection***) in the SMP to the PI input to the integration network. Altering the weighting in the this manner rather than by scaling the VH input independently allows the VH dominate the integrated output at the site with high visual familiarity and even with a large home vector (strong PI cue will be dramatically decreased by TN at familiar site).

Figure 3C shows the initial headings produced by the model replicates the trends reported by ***Wystrach et al.*** (***2015***) and ***Legge et al.*** (***2014***) when the uncertainty of PI and VH cues were altered in a cue-conflict experiments. This leads to improved navigation performance over either PI or VH models independently following a displacement as demonstrated in ***Figure 3***D with the combined model initially following predominantly the home-vector direction before switching to visual homing when the home-vector length drops leading back to the to the familiar route. Again upon encountering the route the model is unable to distinguish the direction in which to travel and hence meanders around the valley of familiarity along the route.

Route Following in the Insect Brain

The above described model can guide insects back to their familiar route area, but lacks the means to recover the route direction upon arrival as observed in homing insects. This is not entirely surprisingly as visual homing relies upon translationally-varying but rotational-invariant information whereas route re-allignment requires rotationally-variant information. Thus we introduce a new elemental guidance system that makes use of the rotationally-varying *phase* coefficients of the frequency information derived from the panoramic skyline which track the orientation of specific features of the visual environment in a similar manner to the bar following head-direction cells reported in fruit flies (***Seelig and Jayaraman, 2015***). Alignment of the current *phase* information, with that experienced when travelling along the habitual route, will thus recover the route direction.

Given the novelty of this method there is little neuroanatomical information on which to base the model architecture. We therefore train a 3-layer artificial neural network (ANN) to associate the same 81 rotational-invariant input neurons used in the VH model with the rotational varying *phase* value of single frequency coefficient experienced when travelling along the habitual route and represented as an 8 neuron-ring encoding. The same steering network as above compares the current heading, but now representing a terrestrial compass rather than celestial compass, to the desired heading provided by the ANN (see ***Figure 4***A and Methods ***subsubsection*** for detailed model description). We speculate that the most likely neural pathway for the RF desired heading is from Optic Lobe via Anterior Optic Tubercle (AOTu) and Bulb to EB(CBL) of the CX (***Homberg et al., 2003***), whereas current heading is likely to pass from Optic Lobe via Posterior Optic Tubercle (POTu) to the PB (***Beetz et al., 2015***) (see ***Figure 4***A).

The route following model accurately replicates the initial paths of real ants in ***Wystrach et al.*** (***2012***) (***Figure 4***B, insert) when released at the start of a familiar route, and the extended paths closely resemble those of real zero vector ants (***Kohler and Wehner, 2005***; ***Mangan and Webb, 2012***) (***Figure 4***B). The quiver plot plotted in the background of ***Figure 4***B show the preferred homing direction output by the ANN when rotated on the spot across locations in the environment. The noise in the results is due to errors in the tracking performance (see examples ***Figure 4***B right) yet as these errors are in largely confined to the magnitude, the steering circuit still drives the ant along the route. The displaced routes also highlight the danger of employing solely RF techniques

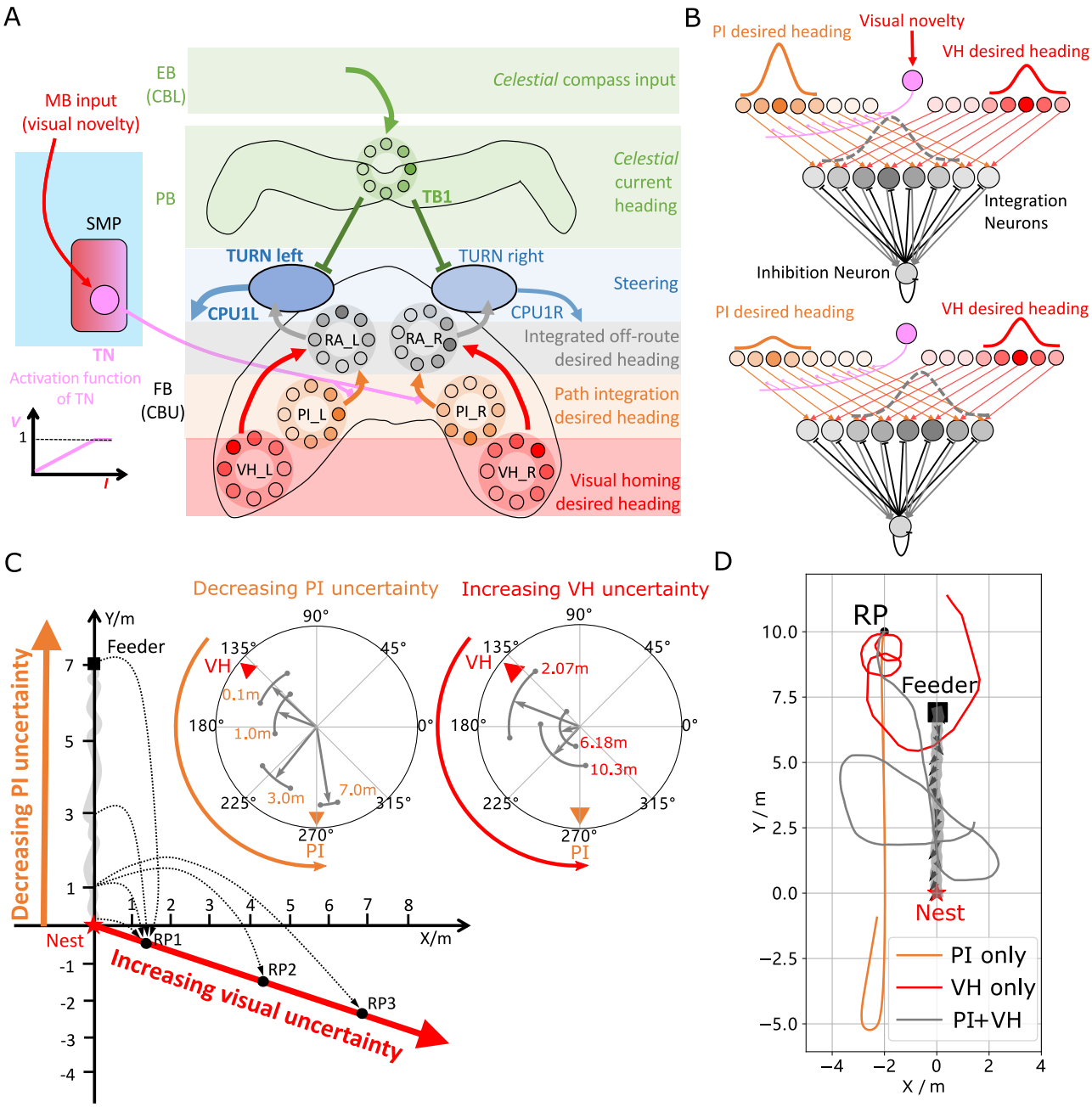

Figure 3. Optimal cue integration in the CX. (**A**) Proposed model for optimally integrating PI and VH guidance systems. In each hemisphere, RAs receive the corresponding inputs from PI and VH and then the outputs are send to the corresponding steering neurons (CPU1 left/right) to generate the final combined motor command. The integration is tuned by the visual novelty activated tuning neuron (TN) whose activation function is shown beside. (**B**) Ring attractor networks optimally integrates PI and VH desired headings. Two examples with different PI cues are presented. The stable state of the integrating neurons in the ring attractor network will optimally integrates the input cues according to their strengths. (**C**) Replication of optimal integration studies. Two sets of simulations are undertaken to test if the model can optimally integrate cues. The grey curve along the y-axis is the trained route, after training the agents are released at different release points (RP1, RP2 and RP3). For the first experiment (benchmark study - ***Wystrach et al.*** (***2015***)), all the agents with different home vector length (i.e., with different PI certainty, generate by manually generate the PI desired heading, for details see ***subsection***) are released at RP1 (i.e., with the same visual novelty and thus visual certainty), the results of initial headings are shown in the left polar plot. For the second experiments (benchmark study - ***Legge et al.*** (***2014***)), the agents with the same home vector length are respectively released at RP1, RP2 and RP3. The results of the initial heading are shown in the right polar plot. (**D**) Typical homing paths of the independent and combined guidance systems.

Figure 3–Figure supplement 1. The extended homing paths and the PI memory in the simulations

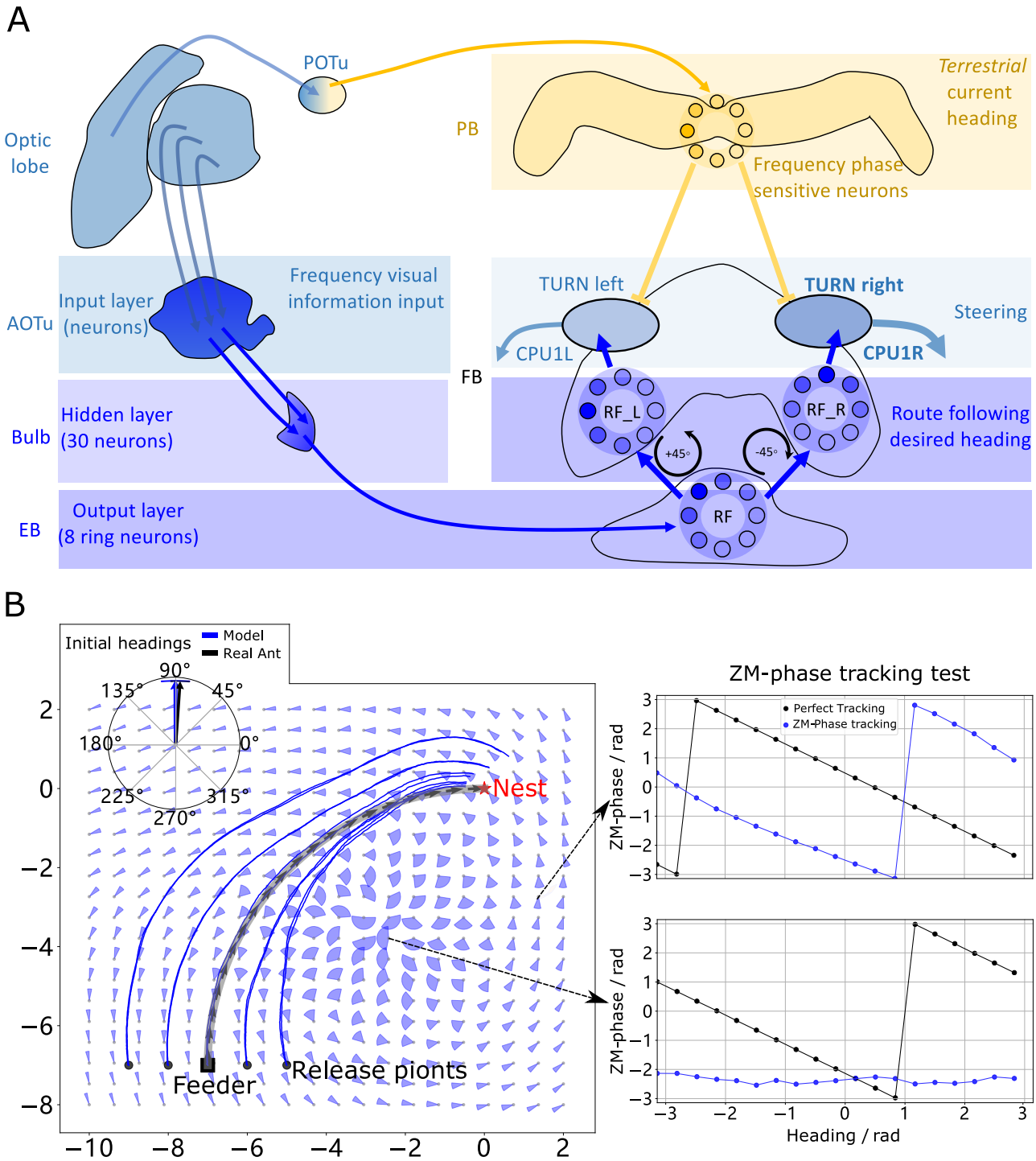

Figure 4. The route following model and performances.(**A**) Proposed model of route following in the insect brain. The visual pathway from the optic lobe via Aotu and Bulb to EB of CX is a fully connected artificial neural network (ANN) with one hidden layer. The input layer receive the magnitudes of the frequency encoded information (the same as the inputs of MB network for VH), the output layer is a 8-neuron ring whose population encoding represents the desired heading of RF. (**B**) Resultant route following behaviours. The blue curves show the homing route of agents released at 5 different release points driven by RF. The fan-plots at the meshed points indicate the circular statistics of the RF model recommended homing directions with 20 different initial headings. The blue and black arrow in the inserted polar plot shows the initial headings of the real (***Wystrach et al., 2012***) and simulated ants released on route $(-7, 0)$ respectively. The plot from up to bottom on the right are two examples of the performance of the ZM-phase tracking at location $(1.5, -3)$ and $(-2.5, -3.5)$ respectively.

which shadow rather than converge with the route in most scenarios, further demonstrating the necessity for integration with the Off-Route strategies that ensure route convergence and subsequent maintenance.

Route Recovery Through Context-Dependent Modulation of Guidance Systems

Homing insects readily recognise familiar route surroundings, recover their bearing, and retrace their habitual path home, irrespective of the status of other guidance system such as PI. Replicating such context-dependent behavioural switching under realistic conditions is the final task for the proposed unified model. The visual valance measured by the MBON provides an ideal signal for context switching with low output when close to the route when RF should dominate versus high output further away from the route when PI and VH should dominate (see ***Figure 2***C). Also the fact that off-route strategies (PI and VH) compute their turning angles with reference to the celestial compass whereas the on-route strategy is driven with reference to a terrestrial compass provides a means to modulate their impact on the steering circuit independently. This is realised through a non-linear weighting of the on-route and off-route strategies which we propose acts through the same SMP pathway as the VH model (see the SN1 and SN2 neuron in ***Figure 5***A).

Figure 5B shows example paths of simulated ants when released sidewards of their habitual route with and without access to their PI system, i.e., the full vector and zero vector agent. Zero-vector agents apply VH to approach the route directly as in ***Figure 5***B but upon arrival switch to RF which guides them home along their habitual path. Full-vector ants initially combine PI and VH making them move parallel to the route direction initially, but again as they approach the familiar route area they switch to RF which guides them back to the nest by the habitual path. Taken together, the proposed unified navigation model successfully clearly fulfils all of the criteria defined for replication of key adaptive behaviour observed in insects (***Figure 1***A).

Discussion

This work addresses two gaps in the current understanding of insect navigation: what are the core visual guidance systems required by the insect navigational toolkit? And how are they coordinated by the insect brain?

We propose that the insect navigation toolkit (***Wehner, 2009***; ***Webb, 2019***) should be extended to include independent visual homing (VH) and route following (RF) systems (see ***Figure 1***B for updated Insect Navigation Toolkit). We show how VH and RF can be realised using frequency-encoding of panoramic skylines to separate information into rotationally-invariant **magnitudes** for VH and rotationally-varying *phases* for RF. Behavioural studies support the use of spatial frequency by bees (***Horridge, 1997***; ***Lehrer, 1999***), with neurons in the lobulla found to have receptive fields akin to basis functions (***O'Carroll, 1993***; ***James and Osorio, 1996***) providing a mechanism by which the optic lobes could extract frequency information. Follow-on modelling of the optic lobe based on the above data is therefore required to extend the neural pathway from sensory input to motor output. We note that ***Gkanias et al.*** (***2019***) recently presented a plausible neural model of the celestial compass processing pipeline that could be easily integrated into the unified model to complete the entire model pathway.

Visual homing is modelled on neural circuits found along the optic lobe, MB, SMP pathway (***Ehmer and Gronenberg, 2002***; ***Gronenberg and López-Riquelme, 2004***) before terminating in the CX steering circuit (***Stone et al., 2017***) and shown capable of producing realistic homing paths. In this schema the MBs do not measure rotationally-varying sensory valence as used to replicate RF (***Ardin et al., 2016***; ***Müller et al., 2018***), but rather the spatially varying (but rotationally-invariant) sensory valence more suited to gradient descent strategies such as visual homing (***Zeil et al., 2003***) and other taxis behaviours (***Wystrach et al., 2016***). This is inline with the hypothesis forwarded by ***Collett and Collett*** (***2018***) that suggest that the MBs output "whether" the current sensory stimulus is positive or negative and the CX then adapts the animal heading, the "whither", accordingly. Conceptually this flexible mechanism has the potential to play a key role realising other navigation

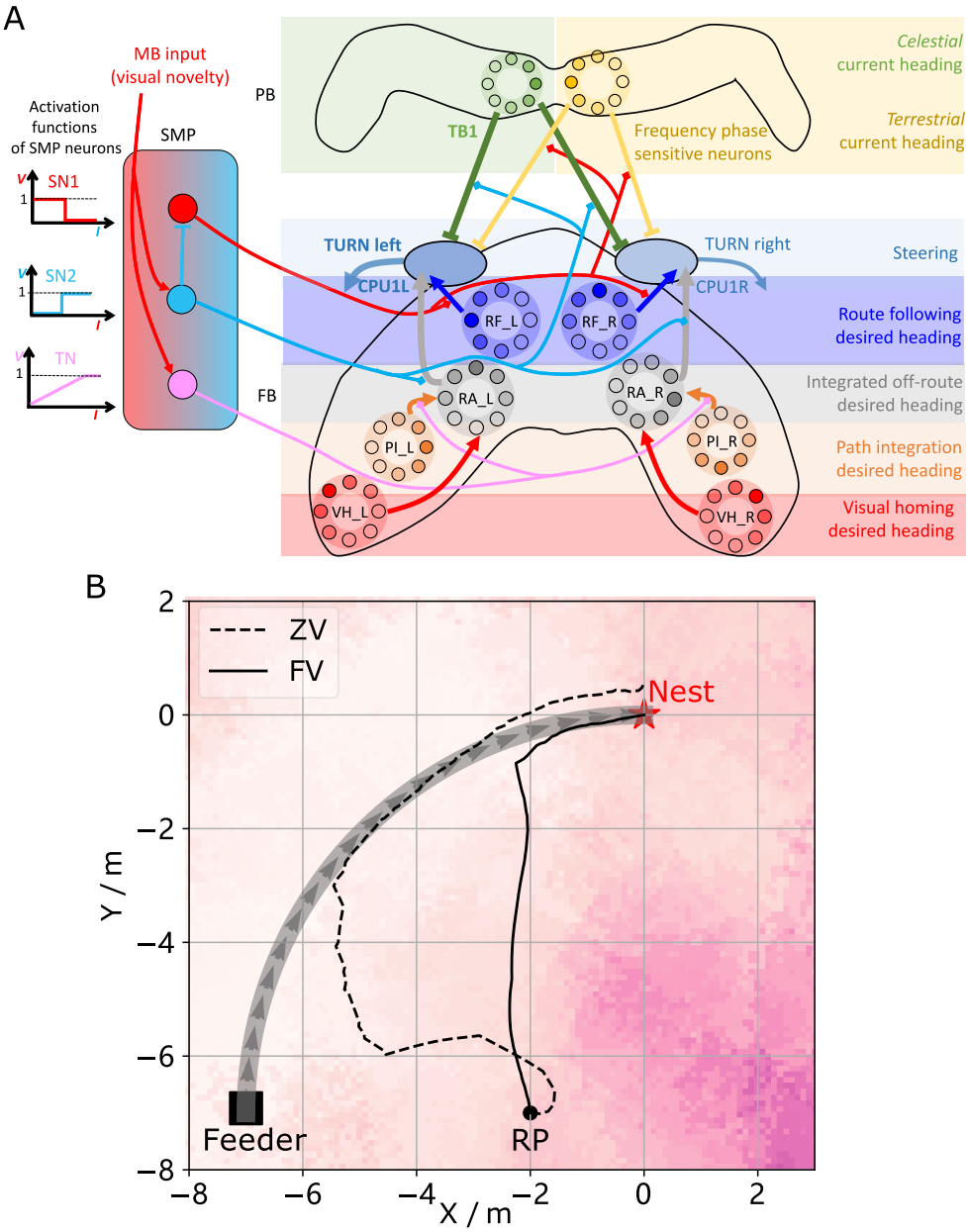

Figure 5. Final Unified model including context-dependent behavioural switching allows for route recovery. (**A**) The final model realising the full array of coordinated navigational behaviours in the insect brain. The coordination are modelled as three neurons in SMP: switching neuron 1 (SN1) and switching neuron 2 (SN2) has mutual exclusive firing state so they work together to switch on/off the output from the on-route RF or off-route PI+VH integrated cue and the celestial/terrestrial current heading to the steering neurons depending on the visual novelty from the MB; The tuning neuron (TN) is the same in ***Figure 3***. The activation functions of these neurons are shown in the left side of SMP box. (**B**): Reproduce the desired homing behaviours of the insect navigation in ***Figure 1***A, dashed curve depicts the non-linear weighting of on and off-route strategies (i.e., VH and RF) for zero vector (ZV) agent and solid curve shows the optimal weighting of the off-route strategies (i.e., PI and VH) and then successfully retrace the habitual route and do RF for the full vector (FV) agents.

behaviours from straight line following (***El Jundi et al., 2016***) to migrations (***Reppert et al., 2016***) as well as more nuanced strategies that flexibly use directional cues from different sensory modalities (***Wystrach et al., 2013***; ***Schwarz et al., 2017***; ***Dacke et al., 2019***).

Route following is shown possible by learned associations between the **magnitudes** (i.e. the place) and the *phase* (the orientation) experienced along a route, allowing reallignment when later

at a proximal location. Neurophysiological evidence suggests that the layered visual pathway from Optic lobe via AOTu and Bulb to the EB of the CX (***Barth and Heisenberg, 1997***; ***Homberg et al., 2003***; ***Omoto et al., 2017***) with its known neural plasticity properties (***Barth and Heisenberg, 1997***; ***Yilmaz et al., 2019***) a possible neural pathway but further analysis is needed to identify the circuit structures that might underpin route following. The RF model developed suggests that the "terrestrial" compass recently discovered in insects (***Seelig and Jayaraman, 2015***) could be driven by extracted *phase* properties of the visual scene.

Closed-loop behavioural studies during which the spatial frequency information of views is altered (similar to ***Paulk et al.*** (***2015***)) coincident with imaging of key brain areas (***Seelig and Jayaraman, 2013***, ***2015***) offers a means to investigate which neural structures make use of what visual information. Complimentary behavioural experiments could verify the distinct VH and RF systems by selectively blocking the proposed neural pathways with impacts on behaviour predicted by ***Figure 2***C and ***Figure 4***B respectively. ***Ofstad et al.*** (***2011***) report that visual homing abilities are lost for fruit flies with a blocked EB of the CX but not MB, which is predicted by our model if animals have learned target facing views to which they can allign. Analysis of the animals orientation during learning is thus vital to unpicking precisely how the above results arise.

With the elemental guidance strategies defined, we propose that their outputs are coordinated through the combined action of the MBs and CX. Specifically, we demonstrate how ring attractor networks, following neural firing patterns recorded in the CX (***Green et al., 2017***), are sufficient for optimally weighting multiple directional cues from the same frame of reference (e.g. VH and PI are both referenced to the celestial compass). The optimal integration of PI and VH using a ring attractor closely matches the networks theorised to govern optimal directional integration in mammals (***Jeffery et al., 2016***) and supports hypothesis of their conserved use across animals. Optimality is secured either through adapting the shape of the activity profile of the input as is the case for PI which naturally scales with distance, or by using a standardised input activity profile with cross-inhibition of competing cues as is the case for VH in the model. The later schema avoids the need for ever increasing neural activity to maintain relevance. This assemblage recreates optimal integration of VH and PI in experimental conditions, and supports recent hypothesis that the CX is the navigation coordinator of insects (***Heinze, 2017***; ***Honkanen et al., 2019***) yet it does not easily extend to allow integration of directional cues from other frames of reference (e.g. Route Following referenced to the terrestrial compass). Indeed as CX steering network seeks to minimise the difference between a current and desired heading, merging input signals from different frames of reference would require similar integration of their respective compass systems.

Rather, the unified model incorporates a context-dependent non-linear switching mechanism to completing alternate between strategies. In the specific case above, as insects approach their familiar terrain the MBs output drops, switching from celestial compass referenced VH and PI guidance to terrestrial compass referenced RF. In summary, the adaptive coordination of guidance cues relies not on the CX alone but rather on the both the CX-based RA networks and a context dependent mediating signal from the MB representing the current visual valance. This distributed architecture is reminiscent of mechanisms found in the visual learning of honeybees (***Plath et al., 2017***), supporting the hypothesis that the MB and the CX act together to generate optimal behaviour according to the context.

Methods and Materials

The proposed networks and the simulations are all implemented by Python 3.5 with external libraries-*numpy*, *matplotlib*, *scipy*, *PIL* and *cv2*. The source code of the implementation is available via https://github.com/XuelongSun/InsectNavigationModel.

Simulated 3D world

The environment used in this study is previously made by ***Stone et al.*** (***2018***) adopted from ***Baddeley et al.*** (***2012***). It is a virtual ant world consisting of artificially and randomly generated bushes, trees

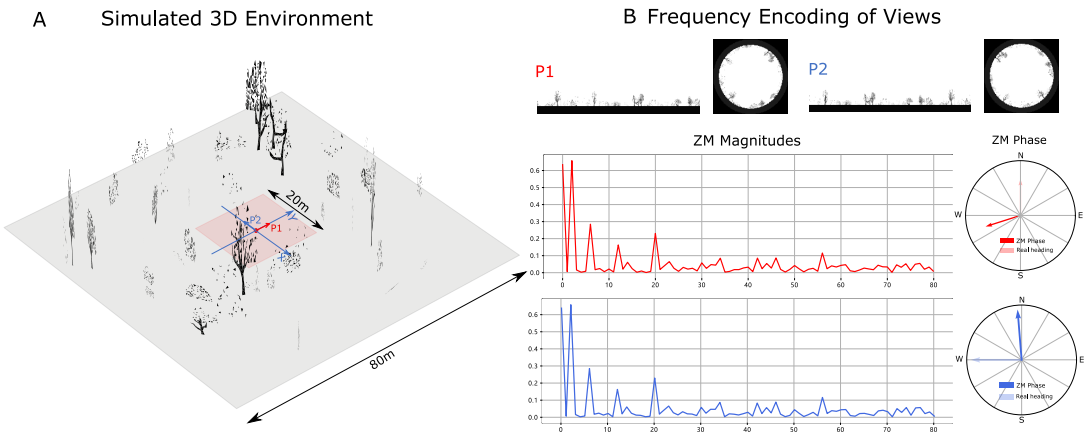

Figure 6. The simulated 3D world and the information provided by the frequency encoding. (A) The simulated 3D world. The pink area with size $20m \times 20m$ is the test zone of our model. Agents are allowed to explore in this obstacle-free world. **(B)**The frequency encoding (Zernike Moment's **magnitudes** and *phase*) of the views sampled from the same location but with different headings (P1 and P2 in **(A)**, with $90°$ heading difference). The first 81 magnitudes are identical while the phase have the difference of about $90°$.

and tussocks based on triangular patches. Therefore, the data of this simulated world is stored in a matrix with the size of $N_P \times 3 \times 3$, defining the three dimensional coordinates of the three vertices of N_P (number of patches) patches. A test area with size $20m \times 20m$ was selected specifically to meet the condition that there is no obstacles, so the agent can freely explore in that area (see ***Figure 6***A).

Image processing

The agent's visual input at location (x, y) with the heading direction θ_h is reconstructed from a point with 1cm height from the ground plane. The filed of view is $360°$ and $90°$ for the horizontal and vertical direction respectively. Then the reconstructed image with size of 300×104 is wrapped into a sky-centred disk with the size of $(104 \times 2) \times (104 \times 2)$ before being converted into the frequency encoded representation (see ***Figure 6***B).

Frequency encoding - Zernike Moment

Zernike Moments (ZM) are defined as the projection of function onto an orthogonal basis polynomials called Zernike polynomials (***Teague, 1980***; ***Khotanzad and Hong, 1990***). This set of functions are defined on the unit circle with polar coordinates (ρ, θ) showed as:

$$V_{nm}(\rho, \theta) = R_{nm}(\rho)e^{jm\theta} \tag{1}$$

Where $n \in N^+$ is the order and m is the repetition meeting the condition: $m \in N$, $|m| \leq n$ and $n - |m|$ is even to get the rotational invariant property. $R_{nm}(\rho)$ is the radial polynomial defined as:

$$R_{nm}(\rho) = \sum_{s=0}^{n-|m|/2} (-1)^s \frac{(n-s)!}{s!(\frac{n+|m|}{2} - s)!(\frac{n-|m|}{2} - s)!} \rho^{n-2s} \tag{2}$$

For a continuous image function $f(x, y)$, the ZM coefficient can be calculated by:

$$Z_{nm}(\rho) = \frac{n+1}{\pi} \int\int_{x^2+y^2 \leq 1} f(x, y) V^*_{nm}(\rho, \theta) dx dy \tag{3}$$

For a digital image, summations can replace the integrals to get the ZM:

$$Z_{nm}(\rho) = \frac{n+1}{\pi} \sum_x \sum_y f(x, y) V^*_{nm}(\rho, \theta), \qquad x^2 + y^2 \leq 1. \tag{4}$$

The image used to calculated the ZM as the input of the visual navigation model is the wrapped format of the reconstructed image (***Figure 6***B) whose centre is taken as the origin of the polar

coordinates, so all the valid pixels are within the unit circle. For a given image I (P1 in ***Figure 6***B) and the rotated version of this image I^{θ_r} (P2 in ***Figure 6***B), the magnitude $A = |Z|$ and phase $\Phi = \angle Z$ of ZM coefficients of these two images will satisfy:

$$\begin{cases} |Z_{nm}^{\theta_r}| = |Z_{nm}e^{-jm\theta_r}| = |Z_{nm}| \quad i.e., \quad A_{nm}^{\theta_r} = A_{nm} \\ \Phi_{nm}^{\theta_r} = \Phi_{nm} - m\theta_r \end{cases} \tag{5}$$

From which we can see that the magnitude of ZM coefficient is keeping the same while the phase of ZM carries the information of rotation (see ***Figure 6***B). This property is the cornerstone of the visual navigation model where the magnitudes (amplitudes) encode the features of the view (see the heat map of ***Figure 6***C) while the phase defines the terrestrial compass (see the quiver plot of ***Figure 6***C).

For the inputs of the VH model, as the ZM with different orders n encode the information of different frequency of the image, in order to cover all the information within the image we set $n = 0$ to $n = 16$. From ***Equation 1*** we know that $V_{n,m} = V_{n,-m}$, so we only let $m \in N^+$ to reduce the computational cost, which overall result in totally $N_{ZM} = (16 \div 2 + 1)^2 = 81$ number of ZM coefficients fed into the visual navigation network. For training the ANN network for RF, in ***Equation 5***, if we set $m = 1$, then we have $\Phi_{n,1}^{\theta_r} = \Phi_{n,1} - \theta_r$ which means that how much the image was rotated from the original image, the same amount of angle will shifted in the phase of the ZM coefficients. Therefore, when the agent compare the magnitudes of ZM of the current view with that of the memorised view, the turn angle that the agent should make to align with the visual memory equals the angular difference of the ZM's phase, i.e. :

$$\Phi_{7,1}^{current} - \Phi_{7,1}^{memory} = \theta_h - \theta_m \tag{6}$$

Where the order n of this ZM is selected to be $n = 7$ manually by comparing the performances with different orders in this specific virtual environment, θ_h is the current heading of the agent while θ_m is the memorised heading direction.

Neural Networks

We use the simple firing rate to model the neurons applied in this proposed networks, where the output firing rate C is a sigmoid function of the input I if there is no special note. In the following descriptions and formulas, a subscript is used to represent the layers or name of the neuron while the superscript is used to represent the value at a specific time or with a specific index.

Celestial current heading

The compass neural network applied in this study is the same as that of ***Stone et al.*** (***2017***), which has three layers of neurons: TL-neurons, CL1-neurons and TB1-neurons. The 16 TL-neurons response to the polarised light and directly modelled as:

$$I_{TL} = \cos(\theta_{TL} - \theta_h) \tag{7}$$

Where $\theta_{TL} \in \{0, \pi/4, \pi/2, 3\pi/4, \pi, 5\pi/4, 3\pi/2, 7\pi/4\}$ representing 8 cardinal directions is the angular preference of the 8 TL-neurons in each hemisphere of the insect brain. The 16 CL2-neurons are inhibited by TL-neuron activity which invert the polarisation response:

$$I_{CL2} = 1.0 - C_{TL} \tag{8}$$

The 8 TB1-neurons act as a ring attractor creating a sinusoidal encoding of the current heading. Each TB1-neuron receives excitation from the CL1-neuron sharing the same directional preference and the inhibitions from other TB1-neurons via the mutual connections:

$$W_{TB1}^{ij} = \frac{\cos(\theta_{TB1}^{i} - \theta_{TB1}^{j}) - 1}{2} \tag{9}$$

$$I_{TB1}^{t,j} = (1-c)C_{CL1}^{t,j} + c\sum_{i=1}^{8} W_{TB1}^{ij} C_{TB1}^{t-1,j} \tag{10}$$

Where c is a balance factor to modify the strength of the inhibition and the CL1 excitation. Finally, the population coding $C_{TB1}^{t,j}, j = 0, 1, ...7$ represents the heading of agent at time t.

MB network and visual homing

The neural network of visual homing is an associative network constrained by the anatomical structure of the mushroom body (MB) of the insects. Differ from ***Ardin et al.*** (***2016***) where a spiking neural network is implemented to model the MB, here we apply a simple version of MB where the average firing rates of neurons are used.

The visual projection neurons (vPNs) directly receive the magnitudes of the Zernike moments coefficients as their firing rates:

$$C^i_{vPN} = A^i, \qquad i = 0, 1, 2...N_{vPN} \tag{11}$$

Where N_{vPN} is the number of the vPN neurons which is the same as the total number of ZM magnitudes applied and in this study $N_{vPN} = N_{ZM} = 81$. The A^i denotes the ith magnitudes of ZM coefficients.

The activation of vPNs are injected into Kenyon cells (KC) through randomly generated binary connections W_{vPN2KC}, which result in the scenario wherein one KC receive 10 randomly selected vPNs' activation:

$$I^j_{KC} = \sum_{i=0}^{N_{vPN}} W^{ji}_{vPN2KC} C^i_{vPN} \tag{12}$$

Where I^j_{KC} denotes the total input current of jth KC from the vPN and the KCs are modelled as binary neurons with the same threshold Thr_{kc}:

$$C_{KC} = \begin{cases} 0 & if \quad I_{KC} \leq Thr_{KC} \\ 1 & if \quad I_{KC} > Thr_{KC} \end{cases} \tag{13}$$

The Extrinsic neuron sums all the activation of Kenyon cells via a plastic connections W_{KC2EN}:

$$C_{EN} = \sum_{i=0}^{N_{KC}} W^i_{KC2EN} C^i_{KC} \tag{14}$$

An anti-Hebbian learning rule is applied for the plasticity of W_{KC2EN} in a simple way:

$$W^t_{KC2EN} = W^{t-1}_{KC2EN} - \eta_{KC2EN} \qquad if \quad C^i_{KC} \geq W^i_{KC2EN} \tag{15}$$

Where η_{KC2EN} is the learning rate. The learning process will happen only when the reward signal is turned on. The activation of EN C_{EN} represents the familiarity of the current view and the change of the C_{EN} is defined as:

$$\Delta C_{EN} = C^t_{EN} - C^{t-1}_{EN} \tag{16}$$

ΔC_{EN} is used to tracking the gradient of the familiarity to guide the agent to the more familiar locations by shifting the TB1 neurons' activation C_{TB1}.

$$C^i_{VH} = C^j_{TB1}, j = \begin{cases} i + offset & if \quad i + offset \leq 7 \\ i + offset - 7 & otherwise \end{cases} \qquad i = 0, 1, ...7 \tag{17}$$

The relationship between the ΔC_{EN} and the $offset$ is shown as following:

$$offset = \begin{cases} 0 & if \quad \Delta C_{EN} < 0 \\ \min(\lfloor k \Delta C_{EN} \rfloor, 4) & otherwise \end{cases} \tag{18}$$

Path integration

The path integration model applied in this paper was published in ***Stone et al.*** (***2017***). The core mechanism of the path integration network is that the CPU4-neurons integrate the activation of TN-neurons that encode the speed of the agent and the reverted activation of TB1-neurons to get the estimation of the home vector. The firing rate of the CPU4 neurons are updated by:

$$I^t_{CPU4} = I^{t-1}_{CPU4} + r(C^t_{TN2} - C^t_{TB1} - k) \tag{19}$$

Where $r = 0.0025$ is the rate of the memory accumulation and $k = 0.1$ is the memory lose. The initial memory charge of CPU4 neurons is set to be $I^0_{CPU4} = 0.1$. The input of the TN2-neurons encoding the speed is calculated by:

$$\begin{cases} I_{TN_L} = [\sin(\theta_h + \theta_{TN})\cos(\theta_h + \theta_{TN})]\boldsymbol{v} \\ I_{TN_R} = [\sin(\theta_h - \theta_{TN})\cos(\theta_h - \theta_{TN})]\boldsymbol{v} \end{cases} \tag{20}$$

where $\boldsymbol{v}$ is the velocity of the agent and θ_{TN} is the preference angle of the TN-neurons. In this study $\theta_{TN} = \pi/4$. Activation function applied to TN2-neurons is rectified linear function:

$$C_{TN2} = \max(0, 2I_{TN}) \tag{21}$$

As CPU4 neurons integrate the speed and direction of the agent, the desired heading of PI can be represented by the population encoding of these neurons, thus:

$$C_{PI} = C_{CPU4} \tag{22}$$

Optimal cue integration

A ring attractor neural network is used to integrate the cues from the VH and PI. As it is reported in ***Hoinville and Wehner*** (***2018***) that by doing vector summation we can get optimal angular cue integration which is the same case as real insects, ***Sun et al.*** (***2018***) gave a biology plausible way to do this kind of computation based on a simple ring attractor neural network. There are two populations of neurons in this network, the first is the combination neurons (CN) which is the output population of the network. Constrained by the number of columns in each hemisphere of the insects brain, we set the number of the CN to be 8, and its firing rate is updated by:

$$\tau\frac{dC_{CN}}{dt} = -C_{CN} + g\left(\sum_{j=1}^{n} W^{ji}_{E\to E}C^j_{CN} + X^i_1 + X^i_2 + W_{I\to E}C_{UI}\right) \qquad i = 0, 1, ...7. \tag{23}$$

Where $W^{ji}_{E\to E}$ is the recurrent connections from j^{th} neuron to i^{th} neuron, $g(x)$ is the activation function endow the non-linear property of the neuron:

$$g(c) = max(0, \rho + c) \tag{24}$$

Where ρ denotes the offset of the function.

In ***Equation 23***, X_1 and X_2 generally denote the cues that should be integrated. In this study, X_1 and X_2 represent the desired heading of path integration (C_{PI}) and visual homing (C_{VH}). The desired heading of PI is also tuned by the tuning neuron (TN) in SMP which receive the activation from the MBON of MB (see ***Figure 2***A) and its activation function is defined by a rectified linear function, i.e.:

$$C_{TN} = \min kC_{EN}, 1 \tag{25}$$

Where k is the scale factor.

Therefore, the X_1 and X_2 for this ring attractor network can be calculated by:

$$\begin{cases} X^i_1 = C_{TN}C^i_{PI} \\ X^i_2 = C^i_{VH} \end{cases} \qquad i = 0, 1, ...7 \tag{26}$$

The second population of the ring attractor is called the uniform inhibition (UI) neurons modelled by:

$$\tau\frac{dC_{UI}}{dt} = -u + g\left(W_{I\to I}C_{UI} + W_{E\to I}\sum_{k=1}^{n} C^k_{CN}\right) \qquad i = 0, 1, ...7. \tag{27}$$

After getting the stable state, the firing rate of the CN neurons in this ring attractor network provides the population encoding of the optimal integrated output C_{OI}:

$$C_{OI} = C_{CN} \tag{28}$$

ANN network and Route Following

The route following model is based on a simple artificial neural network (ANN) with just one hidden layer. The input layer directly takes the magnitudes of the ZM coefficients as the activation in the same way as that of visual projection neurons in MB network. This is a fully connected neural network with the sigmoid activation function, so the forward propagation is ruled by:

$$\begin{cases} Z_l^i = \sum_{i=0}^{N} W^{ji} Y_{l-1}^j \\ Y_i^l = sigmoid(Z_l^i) = \frac{1}{1+e^{-Z_l^i}} \end{cases} \quad i = 0, 1, ...7 \quad and \quad l = 0, 1, 2 \tag{29}$$

Where Z_l^i and Y_l^i denote the input and output of the ith neuron in l^{th} layer, thus the input is same as MB network $Z_0^i = A^i, i = 0, 1, ...N_{ZM}$ and the output of the AIM neural network is consequently the population coding of the RF desired heading, i.e.:

$$C_{RF}^i = Y_i^2 \qquad i = 0, 1, ...7 \tag{30}$$

For a fast and efficient implementation, the learning method applied here is the classical back propagation with gradient descend. The learning rule is not important because what really matters is that this kind of neural network has the ability of relating the image view with the specific heading directions, which can be used by the agent to retrieve the correct heading for homing. The training data are derived from the magnitudes and the population encoded phases of the ZM coefficients of the images reconstructed along a habitual route. The way in which the phase of ZM are encoded in the 8 neuron's population activation is showed as:

$$C_{ZMp} = \cos(\Phi_{7,1} - \theta_{ZMp}) \qquad i = 0, 1, ...7 \tag{31}$$

Where the θ_{ZMp} is the angular preference of the ZM phase sensitive neurons and the C_{ZMp} is the firing rate. Therefore, the training pair for RF network can be defined as $\{A, C_{ZMp}\}$. After training, this network will correlate the desired ZM phase C_{ZMp} with the specific ZM magnitudes A, and when the RF is running, the output of this neural network C_{RF} will represent the desired heading with respect to the current ZM phase represented by the population encoding of the ZM phase sensitive neurons C_{ZMp}.

Steering circuit

The left and right steering neurons ($C_{ST}^i, i = 0, 1, 2...15$) receives the excitation from the desired heading $C_{DH}^i, i = 0, 1, 2...15$ and the inhibition from the current heading $C_{CH}, i = 0, 1, 2...15$ to generate the turning signal:

$$C_{ST}^i = C_{DH}^i - C_{CH}^i \qquad i = 0, 1, ...15 \tag{32}$$

Then, The turning angle here is modelled as the difference of the summation of the activation in different group:

$$\theta_M = (\sum_{i=0}^{7} C_{ST} - \sum_{i=8}^{15} C_{ST}) \tag{33}$$

Where we define that the neurons with index from 0 to 7 is the left group and the neurons with index from 8 to 15 is the right.

In this model, we have two pairs of current heading and desired heading: first, the current heading decoded by C_{TB1} and the desired heading represented by the CN of ring attractor network C_{CN}. Second, the current heading decoded by ZM phase sensitive neuros C_{ZMp} and the desired heading decoded by the output of the RF network C_{RF}. These two groups can be modulated by two switching neurons (SN1 and SN2) in the SMP (***Figure 3***A). These two switch neurons is modelled in a binary way with the step function defined activation function. SN1 will always fire unless SN2 fires while SN2 will keep silent unless the excitation injection from MBON exceeds activation threshold Thr_{SN2} (see ***Figure 5***).

Given that the key part of the steering circuit is the left- and right-shifted inputs from the desired heading injects to the left ($i = 0, 1, ...7$) and right ($i = 8, 9, ...15$) group of the steering neurons respectively, the following equation shows how current heading inputs to the steering circuit are modelled in this paper:

$$\begin{cases} C^i_{CH} = C_{SN1}C^i_{ZMp} + C_{SN2}C^i_{TB1} & (i = 0, 1, ...7), \\ C^i_{CH} = C_{SN1}C^{i-8}_{ZMp} + C_{SN2}C^{i-8}_{TB1} & (i = 8, 9, ...15) \end{cases} \tag{34}$$

And also the inputs of the desired heading:

$$\begin{cases} C^i_{DH} = C_{SN1}C^{i+1}_{RF} + C_{SN2}C^{i+1}_{OI} \quad (i = 0, 1, ...6), \quad C^7_{DH} = C_{SN1}C^0_{RF} + C_{SN2}C^0_{OI} \\ C^i_{DH} = C_{SN1}C^{i-1}_{RF} + C_{SN2}C^{i-1}_{OI} \quad (i = 9, 10, ..15), \quad C^8_{DH} = C_{SN1}C^{15}_{RF} + C_{SN2}C^{15}_{OI} \end{cases} \tag{35}$$

Movement control

From ***Equation 33***, the motion direction θ_M is calculated and thus the simulated animal's velocity $\boldsymbol{v}$ at every step can be computed by:

$$\boldsymbol{v}^t = S_L[\cos\theta^t_M, \sin\theta^t_M] \tag{36}$$

Where S_L is the step length. And then the position of agent $\boldsymbol{P}^{t+1}$ in the Cartesian coordinates for the next step can be calculated by :

$$\boldsymbol{P}^{t+1} = \boldsymbol{P}^t + \boldsymbol{v}^t \tag{37}$$

Reproduce the visual navigation behaviour

The position $\boldsymbol{P}_{R-Arc}$ and heading θ_{R-Arc} alone the arc shape is manually generated by:

$$\begin{cases} \theta^i_{R-Arc} = \frac{\pi}{2} - i\frac{\pi}{2N_M} \\ \boldsymbol{P}^i_{R-Arc} = [-R\sin\theta^i_{R-Arc}, -7 + R\cos\theta^i_{R-Arc}] \end{cases} \quad i = 0, 1..N_M \tag{38}$$

Where the $R = 7m$ is the radius of the arc and $N_M = 20$ in this case is the number of the sampled points (sampled memories) alone the route.

Simulation of visual homing

After training, 12 agents with different initial headings that is evenly distributed in $[-180, 180)$ then be released at the sideway release point ($\boldsymbol{P} = [0, -7]$) for the simulation of VH (***Figure 2***B). The headings of each agent at the position that is 1.5m from the start point is taken as the initial headings.

Simulation of route homing

After training, 2 agents with $0°$ and $180°$ are released at the different release points ($\boldsymbol{P} = [-9, -7]$, $[-8, -7], [-7, -7], [-6, -7], [-5, -7]$) for the simulation of RF (see ***Figure 4***B) to generate the homing path. And then, we release 12 agents on the route ($\boldsymbol{P} = [-7, -7]$) with different initial headings that is evenly distributed in $[-180, 180)$ to compare the results with the real ant data in ***Wystrach et al.*** (***2012***). The heading of each agent at the position that is 0.3m from the start point is taken as the initial headings.

Reproduce the optimal cue integration behaviour

We evaluated the cue integration model by reproducing the results of ***Wystrach et al.*** (***2015***) and ***Legge et al.*** (***2014***). The ants' outbound routes in ***Wystrach et al.*** (***2015***) is bounded by the corridor, so here we simulate the velocity of the agent by:

$$\boldsymbol{v}^t_{out} = [rand(0, 2V_0) - V_0, V_0], \quad t = 0, 1...T_{out} \tag{39}$$

Where the function $rand(0, x)$ generate a random value from the uniform distribution of $[0, x]$, thus the speed of x-axis will be in $[-V_0, V_0]$ and will cancel each other during the forging. The speed of

y-axis is constant so it will accumulated and be recorded by the PI model. And $V_0 = 1cm/s$ is the basic speed of the agent and T_{out} is the total time for outbound phase determining the length of the outbound route. As for the simulated homing route, we duplicate the outbound route when $T_{out} = 700$ but with a inverted heading direction. And then the visual navigation network was trained with images sampled along a simulated route (grey curve in ***Figure 3***B).

Tuning PI uncertainty

The agent in this simulation was allowed to forage to different distances of 0.1m, 1m, 3m or 7m from the nest to accrue different PI states and directional certainties before being translated to a never-before-experienced test site 1.5m from the nest. (RP1 in ***Figure 3***B). For each trial, we release 12 agents with different initial headings that is evenly distributed in $[-180, 180)$. The headings of every agent at the position that is 0.3m from the start point is taken as the initial headings. As in the biological experiment, the angle between the directions recommended by the PI and visual navigation systems differed by approximately $130°$. The initial paths travelled by the simulated ants follow the same pattern as those of real ants under the same experimental manipulation. That is, in the unfamiliar location, route following is suppressed and visual homing and path integration networks compete. As the length of the home vector increase (0.1m -> 7m) the activation of PI memory becomes higher ***Figure Supplement 1***, and will increasingly determine the output of the ring attractor integration. Since the length of the home vector is also encoded in the activation of the PI memory neurons, the ring attractor can extract this information as the strength of the cue. As the visual familiarity is nearly the same in the vicinity of the release point, the strength of visual homing circuit remains constant and has more of an influence as the PI length drops. The resultant behaviour is very close to that observed in real ants and can account for the optimal integration of navigational cues ***Figure 3***B.

Tuning visual uncertainty

The agent in this simulation was allowed to forage to the distances of 1m from the nest to accrue different PI states and directional certainties before being translated to two different release points (RP2 and RP3 in ***Figure 3***B). From RP1 to RP3, the distance from nest is creasing so does the visual uncertainty. For each trial, we release 12 agents with different initial headings that is evenly distributed in $[-180, 180)$. The headings of each agent at the position that is 0.3m from the start point is taken as the initial headings.

Simulation of the whole model

The first simulation (results in ***Figure 5***B) to show the zero-vector agent homing from the sideway release points to the familiar route and then switch to RF use the same habitual route in ***subsection*** . So does the learning process.

The second simulation showing the full-vector agent integrating PI and VH to the familiar sites and then switch to RF uses the large arc-shaped route generated by:

$$\begin{cases} \theta_R^i = \frac{-1\pi}{3} - i\frac{\pi}{2N_M} \\ \boldsymbol{P}_R^i = [-7\sqrt{3} - R\cos\theta_R^i, R\sin\theta_R^i] \end{cases} \quad i = 0, 1..N_M \tag{40}$$

where $R = 14m$ is the radius of the route and $N_M = 20$ is the number of samples. $\boldsymbol{P}_R$ is the position and θ_R is the heading alone the route. The network also trained with the images sampled along the route. The PI memory is generated by letting the agent forage along the route from nest to feeder which decode the home vector of length 14m.

Acknowledgements

This research has received funding from the European Union's Horizon 2020 research and innovation programme under the Marie Sklodowska-Curie grant agreement No 778062, ULTRACEPT and No 691154, STEP2DYNA.

Thanks to the Barbara Webb, Hadi Maboudi, Alex Cope and Andrew Philippedes for comments on early drafts. Also to Antoine Wystrach for provision of data from previous works.

References

Ardin P, Peng F, Mangan M, Lagogiannis K, Webb B. Using an Insect Mushroom Body Circuit to Encode Route Memory in Complex Natural Environments. PLoS Computational Biology. 2016; doi: 10.1371/journal.pcbi.1004683.

Aso Y, Hattori D, Yu Y, Johnston RM, Iyer NA, Ngo TTB, Dionne H, Abbott LF, Axel R, Tanimoto H, Rubin GM. The neuronal architecture of the mushroom body provides a logic for associative learning. eLife. 2014; 3:e04577. doi: 10.7554/eLife.04577.

Baddeley B, Graham P, Husbands P, Philippides A. A model of ant route navigation driven by scene familiarity. PLoS Computational Biology. 2012; doi: 10.1371/journal.pcbi.1002336.

Barth M, Heisenberg M. Vision affects mushroom bodies and central complex in Drosophila melanogaster. Learning & Memory. 1997; 4(2):219–229.

Beetz MJ, el Jundi B, Heinze S, Homberg U. Topographic organization and possible function of the posterior optic tubercles in the brain of the desert locust Schistocerca gregaria. Journal of Comparative Neurology. 2015; 523(11):1589–1607.

Bregy P, Sommer S, Wehner R. Nest-mark orientation versus vector navigation in desert ants. Journal of Experimental Biology. 2008; 211(12):1868–1873.

Cartwright B, Collett T. How honey bees use landmarks to guide their return to a food source. Nature. 1982; 295(5850):560.

Collett M. How navigational guidance systems are combined in a desert ant. Current Biology. 2012; 22(10):927–932.

Collett M, Chittka L, Collett TS. Spatial memory in insect navigation. Current Biology. 2013; 23(17):R789–R800. http://dx.doi.org/10.1016/j.cub.2013.07.020, doi: 10.1016/j.cub.2013.07.020.

Collett M, Collett TS. How does the insect central complex use mushroom body output for steering? Current Biology. 2018; 28(13):R733–R734. http://dx.doi.org/10.1016/j.cub.2018.05.060, doi: 10.1016/j.cub.2018.05.060.

Collett TS. Path integration: how details of the honeybee waggle dance and the foraging strategies of desert ants might help in understanding its mechanisms. Journal of Experimental Biology. 2019; 222(11):jeb205187.

Collett T. Insect navigation en route to the goal: multiple strategies for the use of landmarks. Journal of Experimental Biology. 1996; 199(1):227–235.

Cruse H, Wehner R. No need for a cognitive map: decentralized memory for insect navigation. PLoS computational biology. 2011; 7(3):e1002009.

Dacke M, Bell AT, Foster JJ, Baird EJ, Strube-Bloss MF, Byrne MJ, el Jundi B. Multimodal cue integration in the dung beetle compass. Proceedings of the National Academy of Sciences. 2019; p. 201904308.

Dewar ADM, Philippides A, Graham P. What is the relationship between visual environment and the form of ant learning-walks? An in silico investigation of insect navigation. Adaptive Behavior. 2014; 22(3):163–179. https://doi.org/10.1177/1059712313516132, doi: 10.1177/1059712313516132.

Ehmer B, Gronenberg W. Segregation of visual input to the mushroom bodies in the honeybee (Apis mellifera). Journal of Comparative Neurology. 2002; 451(4):362–373.

El Jundi B, Foster JJ, Khaldy L, Byrne MJ, Dacke M, Baird E. A snapshot-based mechanism for celestial orientation. Current biology. 2016; 26(11):1456–1462.

Fleischmann PN, Christian M, Müller VL, Rössler W, Wehner R. Ontogeny of learning walks and the acquisition of landmark information in desert ants, Cataglyphis fortis. Journal of Experimental Biology. 2016; 219(19):3137–3145.

Fukushi T, Wehner R. Navigation in wood ants Formica japonica: context dependent use of landmarks. Journal of Experimental Biology. 2004; 207(19):3431–3439.

Gkanias E, Risse B, Mangan M, Webb B. From skylight input to behavioural output: a computational model of the insect polarised light compass. PLoS computational biology. 2019; 15(7):e1007123.

Graham P, Philippides A, Baddeley B. Animal cognition: multi-modal interactions in ant learning. Current Biology. 2010; 20(15):R639–R640.

Green J, Adachi A, Shah KK, Hirokawa JD, Magani PS, Maimon G. A neural circuit architecture for angular integration in Drosophila. Nature. 2017; 546(7656):101.

Gronenberg W, López-Riquelme G. Multisensory convergence in the mushroom bodies of ants and bees. Acta Biologica Hungarica. 2004; 55(1-4):31–37.

Harrison JF, Fewell JH, Stiller TM, Breed MD. Effects of experience on use of orientation cues in the giant tropical ant. Animal behaviour. 1989; .

Heinze S. Unraveling the neural basis of insect navigation. Current Opinion in Insect Science. 2017; 24(Figure 1):58–67. http://dx.doi.org/10.1016/j.cois.2017.09.001, doi: 10.1016/j.cois.2017.09.001.

Heinze S, Homberg U. Maplike representation of celestial E-vector orientations in the brain of an insect. Science. 2007; 315(5814):995–997.

Heinze S, Narendra A, Cheung A. Principles of Insect Path Integration. Current Biology. 2018; 28(17):R1043–R1058. https://doi.org/10.1016/j.cub.2018.04.058, doi: 10.1016/j.cub.2018.04.058.

Heinze S, Pfeiffer K. The insect central complex-from sensory coding to directing movement. Frontiers in behavioral neuroscience. 2018; 12:156.

Heisenberg M. Mushroom body memoir: from maps to models. Nature Reviews Neuroscience. 2003; 4(4):266.

Hoinville T, Wehner R. Optimal multiguidance integration in insect navigation. Proceedings of the National Academy of Sciences. 2018; 115(11):201721668. http://www.pnas.org/lookup/doi/10.1073/pnas.1721668115, doi: 10.1073/pnas.1721668115.

Hoinville T, Wehner R, Cruse H. Learning and retrieval of memory elements in a navigation task. In: *Conference on Biomimetic and Biohybrid Systems* Springer; 2012. p. 120–131.

Homberg U, Hofer S, Pfeiffer K, Gebhardt S. Organization and neural connections of the anterior optic tubercle in the brain of the locust, Schistocerca gregaria. Journal of Comparative Neurology. 2003; 462(4):415–430.

Honkanen A, Adden A, da Silva Freitas J, Heinze S. The insect central complex and the neural basis of navigational strategies. The Journal of Experimental Biology. 2019; 222(Suppl 1):jeb188854. doi: 10.1242/jeb.188854.

Horridge GA. Pattern discrimination by the honeybee: disruption as a cue. Journal of Comparative Physiology A. 1997; 181(3):267–277.

James A, Osorio D. Characterisation of columnar neurons and visual signal processing in the medulla of the locust optic lobe by system identification techniques. Journal of Comparative Physiology A. 1996; 178(2):183–199.

Jeffery KJ, Page HJ, Stringer SM. Optimal cue combination and landmark-stability learning in the head direction system. The Journal of physiology. 2016; 594(22):6527–6534.

Khotanzad A, Hong YH. Invariant image recognition by Zernike moments. IEEE Transactions on pattern analysis and machine intelligence. 1990; 12(5):489–497.

Kodzhabashev A, Mangan M. Route following without scanning. In: *Conference on Biomimetic and Biohybrid Systems* Springer; 2015. p. 199–210.

Kohler M, Wehner R. Idiosyncratic route-based memories in desert ants, Melophorus bagoti: how do they interact with path-integration vectors? Neurobiology of learning and memory. 2005; 83(1):1–12.

Legge ELG, Wystrach A, Spetch ML, Cheng K. Combining sky and earth: desert ants (Melophorus bagoti) show weighted integration of celestial and terrestrial cues. Journal of Experimental Biology. 2014; 217(23):4159–4166. http://jeb.biologists.org/cgi/doi/10.1242/jeb.107862, doi: 10.1242/jeb.107862.

Lehrer M. Shape perception in the honeybee: symmetry as a global framework. International Journal of Plant Sciences. 1999; 160(S6):S51–S65.

Mangan M, Webb B. Spontaneous formation of multiple routes in individual desert ants (Cataglyphis velox). Behavioral Ecology. 2012; 23(5):944–954. doi: 10.1093/beheco/ars051.

Müller J, Nawrot M, Menzel R, Landgraf T. A neural network model for familiarity and context learning during honeybee foraging flights. Biological cybernetics. 2018; 112(1-2):113–126.

Müller M, Wehner R. Path integration provides a scaffold for landmark learning in desert ants. Current Biology. 2010; 20(15):1368–1371.

Narendra A. Homing strategies of the Australian desert ant Melophorus bagoti II. Interaction of the path integrator with visual cue information. Journal of Experimental Biology. 2007; 210(10):1804–1812.

O'Carroll D. Feature-detecting neurons in dragonflies. Nature. 1993; 362(6420):541.

Ofstad TA, Zuker CS, Reiser MB. Visual place learning in Drosophila melanogaster. Nature. 2011; 474. doi: 10.1038/nature10131.

Omoto JJ, Keleş MF, Nguyen BCM, Bolanos C, Lovick JK, Frye MA, Hartenstein V. Visual input to the Drosophila central complex by developmentally and functionally distinct neuronal populations. Current Biology. 2017; 27(8):1098–1110.

Paulk AC, Kirszenblat L, Zhou Y, van Swinderen B. Closed-loop behavioral control increases coherence in the fly brain. Journal of Neuroscience. 2015; 35(28):10304–10315.

Pfeiffer K, Homberg U. Organization and functional roles of the central complex in the insect brain. Annual review of entomology. 2014; 59:165–184.

Plath JA, Entler BV, Kirkerud NH, Schlegel U, Galizia CG, Barron AB. Different Roles for Honey Bee Mushroom Bodies and Central Complex in Visual Learning of Colored Lights in an Aversive Conditioning Assay. Frontiers in Behavioral Neuroscience. 2017; 11(May). doi: 10.3389/fnbeh.2017.00098.

Reppert SM, Guerra PA, Merlin C. Neurobiology of monarch butterfly migration. Annual review of entomology. 2016; 61.

Schwarz S, Mangan M, Zeil J, Webb B, Wystrach A. How ants use vision when homing backward. Current Biology. 2017; 27(3):401–407.

Seelig JD, Jayaraman V. Feature detection and orientation tuning in the Drosophila central complex. Nature. 2013; 503(7475):262–266. http://dx.doi.org/10.1038/nature12601, doi: 10.1038/nature12601.

Seelig JD, Jayaraman V. Neural dynamics for landmark orientation and angular path integration. Nature. 2015; 521(7551):186–191. doi: 10.1038/nature14446.

Stone T, Mangan M, Wystrach A, Webb B. Rotation invariant visual processing for spatial memory in insects. Interface Focus. 2018; doi: 10.1098/rsfs.2018.0010.

Stone T, Webb B, Adden A, Weddig NB, Honkanen A, Templin R, Wcislo W, Scimeca L, Warrant E, Heinze S. An Anatomically Constrained Model for Path Integration in the Bee Brain. Current Biology. 2017; 27(20):3069–3085.e11. https://doi.org/10.1016/j.cub.2017.08.052, doi: 10.1016/j.cub.2017.08.052.

Stürzl W, Zeil J, Boeddeker N, Hemmi JM. How wasps acquire and use views for homing. Current Biology. 2016; 26(4):470–482.

Sun X, Mangan M, Yue S. An analysis of a ring attractor model for cue integration. In: *Conference on Biomimetic and Biohybrid Systems* Springer; 2018. p. 459–470.

Teague MR. Image analysis via the general theory of moments. JOSA. 1980; 70(8):920–930.

Touretzky DS. Attractor network models of head direction cells. Head direction cells and the neural mechanisms of spatial orientation. 2005; p. 411–432.

Webb B. The internal maps of insects. The Journal of Experimental Biology. 2019; 222(Suppl 1):jeb188094. doi: 10.1242/jeb.188094.

Wehner R. The architecture of the desert ant's navigational toolkit. Myrmecological News. 2009; 12(September):85–96.

Wystrach A, Beugnon G, Cheng K. Ants might use different view-matching strategies on and off the route. Journal of Experimental Biology. 2012; 215(1):44–55. http://jeb.biologists.org/cgi/doi/10.1242/jeb.059584, doi: 10.1242/jeb.059584.

Wystrach A, Mangan M, Philippides A, Graham P. Snapshots in ants? New interpretations of paradigmatic experiments. Journal of Experimental Biology. 2013; 216(10):1766–1770. doi: 10.1242/jeb.082941.

Wystrach A, Beugnon G, Cheng K. Landmarks or panoramas: what do navigating ants attend to for guidance? Frontiers in Zoology. 2011; 8(1):21.

Wystrach A, Lagogiannis K, Webb B. Continuous lateral oscillations as a core mechanism for taxis in drosophila larvae. eLife. 2016; 5(OCTOBER2016). doi: 10.7554/eLife.15504.

Wystrach A, Mangan M, Webb B. Optimal cue integration in ants. Proceedings of the Royal Society B: Biological Sciences. 2015; 282(1816). doi: 10.1098/rspb.2015.1484.

Yilmaz A, Grübel K, Spaethe J, Rössler W. Distributed plasticity in ant visual pathways following colour learning. Proceedings of the Royal Society B. 2019; 286(1896):20182813.

Zeil J. Visual homing: an insect perspective. Current opinion in neurobiology. 2012; 22(2):285–293.

Zeil J, Fleischmann PN. The learning walks of ants (Hymenoptera: Formicidae). Myrmecological News. 2019; 29.

Zeil J, Hofmann MI, Chahl JS. Catchment areas of panoramic snapshots in outdoor scenes. JOSA A. 2003; 20(3):450–469.

Zeil J, Kelber A, Voss R. Structure and function of learning flights in ground-nesting bees and wasps. Journal of Experimental Biology. 1996; 199(1):245–252.

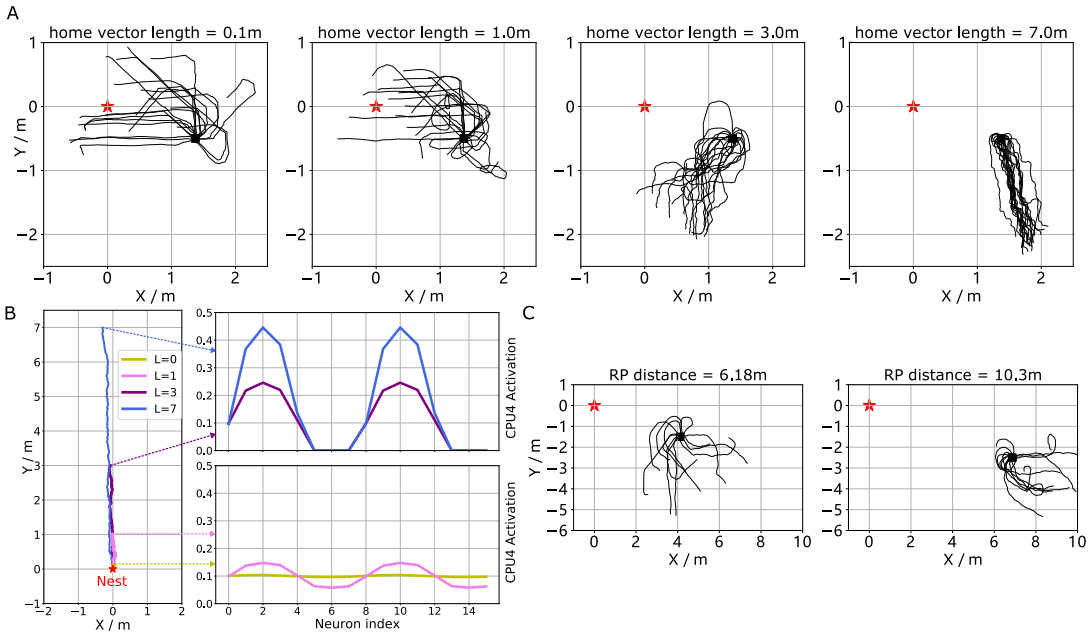

Figure 3–Figure supplement 1. The extended homing paths and the PI memory in the simulations. (A) The extended homing path of 20 agents released at RP1 in Figure 3B with different home vector length. **(B)** The activation of CPU4 neurons (PI memory) encoding home vectors with different lengths from 0 to 7.0m. **(C)** The extended homing paths of 20 agents released at RP2 and RP3 in Figure 3B.